JATIS Journal of Astronomical Telescopes, Instruments, and Systems

RESEARCH PAPER

Multiparameter sensitivity analysis of tilt-to-length coupling noise in Taiji test mass interferometer

Fei Xie[a,b,c] **Xiaodong Peng**,[a,b,d,e] **Wenlin Tang**[b] **Mengyuan Zhao**,[f] **and Xiaoshan Ma**[g,*]

[a]UCAS, Hangzhou Institute for Advanced Study, School of Fundamental Physics and Mathematical Sciences, Hangzhou, China
[b]Chinese Academy of Sciences, National Space Science Center, Key Laboratory of Electronics and Information Technology for Space System, Beijing, China
[c]University of Chinese Academy of Sciences, Beijing, China
[d]Taiji Laboratory for Gravitational Wave Universe, Hangzhou, China
[e]Key Laboratory of Gravitational Wave Precision Measurement of Zhejiang Province, Hangzhou, China
[f]Xi'an University of Finance and Economics, School of Information, Xi'an, China
[g]Chinese Academy of Sciences, Institute of Engineering Thermophysics, National Key Laboratory of Science and Technology on Advanced Light-duty Gas-turbine, Beijing, China

ABSTRACT. Tilt-to-length (TTL) coupling noise is a significant noise source for test mass interferometers in Laser Interferometer Space Antenna or Taiji, but identifying key parameters is a challenge due to the large number of influencing factors and complex interrelationships. Simulation models based on the heterodyne interference process and the signal readout of the test mass interferometer were constructed to generate a dataset containing different parameters and corresponding to the longitudinal path length noise caused by TTL coupling. The eXtreme Gradient Boosting (XGBoost) model was employed to fit the nonlinear relationships between the parameters and TTL coupling noise. Based on the fitting results of the XGBoost model, the sensitivity of single factor and multiple factors was performed using SHapley Additive exPlanation (SHAP) values and attribution value matrix, and the results were validated by the analytical models. Without reducing the fitting accuracy, the parameter dimension was decreased from ~60 to 11 according to sensitivities, retaining those most relevant to angular misalignment. The results showed that the angle of the test mass, the angle of the beam splitters and mirrors, and the lateral offset of the test mass had a significant impact on TTL coupling noise. The introduction of machine learning methods into the study of TTL coupling contributes to a deeper understanding of noise mechanisms and provides references for optimizing the instrument design of the Taiji program.

Keywords: space-based gravitational wave detection; intrasatellite test mass interferometer; tilt-to-length coupling noise; sensitivity analysis

Paper 24151G received Sep. 22, 2024; revised Jan. 1, 2025; accepted Jan. 24, 2025; published Feb. 21, 2025.

1 Introduction

Gravitational wave detection opens a new window for basic physics, astronomy, and cosmology research. The working frequency band of space detection is much lower than that of ground-based detectors such as the Laser Interferometer Gravitational Wave Observatory and therefore attracts increasing attention of scientists from all over the world. Laser interferometry has become

*Address all correspondence to Xiaoshan Ma, maxiaoshan@iet.cn

the first choice for space gravitational wave detection programs, such as Laser Interferometer Space Antenna (LISA),[1] DECi-hertz Interferometer Gravitational-Wave Observatory,[2] TianQin,[3] and Taiji.[4] It involves detecting picometer-level distance variations between free-falling test masses in two spacecraft, allowing for the inference of gravitational wave signals. The split interferometry concept is applied to measure the distance variations between the two test masses, and the measurement is segmented into three parts: the distance variation between the two spacecraft and the distance variations between each test mass and its respective optical bench.[5] Accordingly, inter-satellite and intra-satellite interferometers were designed to measure the above distance variations, also known as scientific and test mass interferometers, separately.

In high-precision space laser interferometric measurement systems, such as those of LISA or Taiji, one significant noise source is the tilt-to-length (TTL), which is the coupling from angular misalignment of an interferometric beam into the length readout of an interferometer.[6] For the Taiji program, TTL noise is present in both inter-satellite and intra-satellite interferometers. In the case of scientific interferometers, TTL coupling primarily occurs due to mutual motion between satellite systems. Wegener et al.[7] characterized TTL coupling noise in laser interferometers using coupling factors and estimated the spacecraft's center of mass relative to the interferometer reference point's nadir and cross-track components based on coupling factor parameters. Sasso et al.[8] analyzed the coupling between wavefront errors and jitter, misalignments, and aberrations in interfering wavefronts.[9] Telescopes in scientific interferometers are used to emit and receive laser beams, and TTL coupling in the interferometer primarily occurs due to angular fluctuations between the beams received from distant spacecraft and the local spacecraft. Therefore, research related to telescope jitter and wavefront aberration has been conducted.[10,11] Recent research has focused on TTL coupling noise induced by satellite attitude change, telescope manufacturing processes, assembly errors, and alignment errors in intersatellite interferometer systems.[12–14]

For the test mass interferometer, TTL coupling primarily occurs due to tilting and jitter of optical components and test masses. Tröbs et al.[15] reduced the TTL coupling noise of the test mass interferometer by designing an imaging system; they conducted simulations to analyze the sensitivity of the beam parameters and verified the results through theoretical calculations and experiments. Hartig and Wanner[16] proposed an analytical model of the TTL coupling noise of the LISA Pathfinder (LPF) and found that TTL coupling occurs mainly due to changes in the relative position of the test mass. Armano et al.[17] proposed two TTL coupling models of the LPF and verified them using experimental data to explain the dependence of TTL coupling on the test mass alignment angle, providing a comprehensive understanding of TTL coupling in the LPF. Ideally, the test mass moves along the geodesic line. However, the test mass is inevitably subjected to a variety of disturbances that result in dynamic changes in its position and attitude. The TTL coupling noise caused by these variations is the focus of recent research.[18,19]

The research above indicates that there are many factors influencing TTL coupling noise and noise exhibiting complex linear and nonlinear relationships. Identifying and selecting the key parameters that have the most significant impact on system performance is challenging, posing difficulties to system design. Based on the composition of the interferometry system and the preliminary optical path of the test mass interferometer for the Taiji program,[20] this work aims to investigate TTL coupling of the test mass interferometers. Through Gaussian beam tracing, the propagation of laser beams through optical setups is simulated, and the interferometer signals are computed. The TTL coupling noise caused by tilt and the jitter of the optical components and test masses are simulated. A typical machine learning model, eXtreme Gradient Boosting (XGBoost),[21] is employed to fit the nonlinear relationship between the influencing parameters and TTL coupling noise. The method is able to synthesize coupling relationships under multiple influences without losing computational efficiency. Crucial parameters of the interferometer are identified by sensitivity analysis, thus providing useful reference and support for the optimal design of the interferometer of the Taiji program.

2 Basic Theory

The two interfering beams are modeled as fundamental mode Gaussian beams, and the complex amplitude of the electric field is calculated as

$$E(\mathbf{r},z) = E_0(z)\exp\left\{-i\phi_{\mathrm{ac}} + i\eta(z) - i\frac{k}{2}\mathbf{r}^T Q\mathbf{r}\right\}, \tag{1}$$

where $E_0(z)$ represents the normalization constant, φ_{ac} represents the accumulated phase, $\eta(z)$ represents the Gouy phase, k represents the wavenumber, Q represents the complex radius of the curvature tensor for generalized Gaussian beams, and the superscript T means transposed.

The complex amplitude of the electric field due to the heterodyne interference of the two beams at the detector can be computed as the integral of the product of the electric field of the measurement beam and the complex conjugated electric of the reference beam on the surface of the detector, which is calculated as

$$C = \int \mathrm{d}A(E_m E_r^*), \tag{2}$$

where A represents the detector surface, m represents the measurement beam, and r represents the reference beam. For the heterodyne measurement, quadrant photodiodes (QPDs) are often used, which consist of four individual photosensitive segments that can be read out separately. Therefore, there are four finite integrals to be performed, resulting in four complex amplitudes and consequently four interferometric outputs. Using the definition in LPF, the longitudinal path-length signal (LPS) can be calculated by combining the four outputs as follows:[6]

$$\mathrm{LPS}_{\mathrm{LPF}} = \frac{1}{k}\arg(C_A + C_B + C_C + C_D), \tag{3}$$

where A, B, C, and D represent the four quadrants of the QPD.

For space-based gravitational wave laser interferometry measurement systems, the LPS output by the interferometer includes not only distance changes caused by gravitational waves but also inevitably the noise generated by various factors or effects, such as shot noise and TTL coupling noise. Studying TTL coupling noise is to establish and analyze the LPS caused by factors related to angular misalignment. Nongeometric and geometric factors both cause TTL coupling noise, which can be expressed as follows:[22]

$$\mathrm{LPS} = \mathrm{OPD} + \mathrm{LPS}_{\mathrm{ng}}, \tag{4}$$

where optical path length difference (OPD) represents the TTL coupling noise caused by geometric factors and $\mathrm{LPS}_{\mathrm{ng}}$ represents the TTL coupling noise caused by nongeometric factors. The geometric factor OPD includes the lever arm effect and piston effect.[19] The lever arm effect refers to the change in the geometric path length caused when one beam is tilted by an angle around a pivot. The piston effect refers to the effect where a tilt of the test mass (or mirror) causes a longitudinal movement of the reflective surface due to an offset between the pivot point and the reflective surface. The nongeometric factors of $\mathrm{LPS}_{\mathrm{ng}}$ include the beam offset, beam parameters, signal definition, wavefront errors, and factors inherent to the detector itself.[22]

3 Methodology

In this section, the heterodyne interference process and the signal readout of the test mass interferometer are modeled, and the TTL-coupled noise with different influencing factors is simulated to form a database. Subsequently, the XGBoost model is utilized to fit the nonlinear relationships between the parameters and noise. Finally, the SHapley Additive exPlanation (SHAP) model is incorporated for sensitivity analysis.

3.1 Simulation Model and Dataset

In addition to laser and detector, the high-precision laser interferometric systems for space gravitational wave detection are configured with a number of optical components, such as lenses, beamsplitters, and mirrors. According to the preliminary design of the interferometer for the Taiji program,[20] an ideal test mass interferometer was established, shown in Fig. 1, to simulate and analyze the TTL coupled noise. The exact coordinates and normal vectors of the optical components are in Table 1, and the coordinates of reference beam (RB) and measurement beam (MB) represent the origins of the two beams. The relative position of the test mass and the optical bench, along with the angle definitions of the test mass, are shown in Fig. 2.

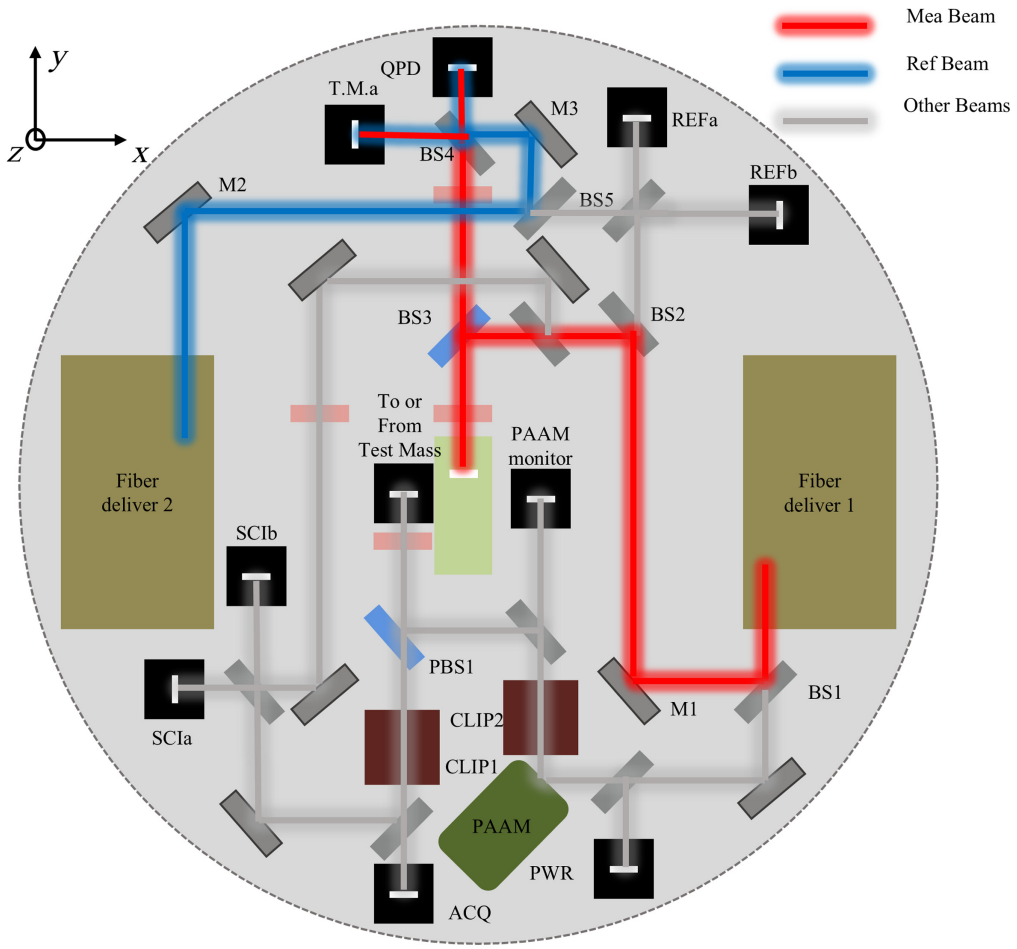

Fig. 1 Schematic diagram of the test mass interferometer.[20] The beam shown in red is the measurement beam used for the test mass interferometer, whereas the blue beam serves as the reference beam. Beam for other interferometers, shown in grey. The gray circular base is an optical bench with the center point of the optical bench as the coordinate origin and the stage normal vector as the *z*-axis. Its *x*- and *y*-axes are shown in the upper left of the figure solely to indicate direction. The reference beam is emitted from fiber deliver 2(F2), reflected by mirror 2 (M2), beam splitter 5 (BS5), mirror 3 (M3), and beam splitter 4 (BS4) and finally reaches the QPD. The measurement beam is generated by fiber deliver 1(F1), reflected by the beam splitter 1 (BS1), mirror 1 (M1), beam splitter 2 (BS2), beam splitter 3 (BS3), and test mass and then reaches the QPD through beam splitter 3 (BS3) and beam splitter 4 (BS4), interfering with the reference beam.

We have fully considered the factors that may cause TTL coupling noise in the test mass interferometer and designed models to simulate the heterodyne interference process and calculated the output of the interferometer. The simulation flowchart is shown in Fig. 3. First, the simulation start time and number of steps are set. Then, the parameters of the optical platform are set. TTL coupling noise is introduced by varying the waist radius and waist positions of the beam, setting beam offsets, adjusting the radius and slit size of the QPD detector, and varying the coordinates and attitudes of optical components and the test mass. Next, the measurement beam and reference beam are modeled as fundamental Gaussian beams characterized by the q-parameter. Gaussian beam tracing models the laser beam as a combination of its beam axis and the q-parameter. The beam axis is traced through the components in the interferometer by means of geometrical optics, whereas the beam propagation is achieved through the transformation of the q-parameter according to the well-known ABCD law for paraxial optical systems. The beam axis is traced up to the final surface, QPD, to compute the complex amplitude of the electric field due to the heterodyne interference by performing Eq. (2). Finally, the LPS is extracted according to Eq. (3).

Table 1 List of the optical components of the test mass interferometer.

Item		Center coordinates			Normal vector coordinates		
Abbreviations	Description	x	y	z	x	y	z
F1	Fiber deliver 1	117.4	0.5	0	0	−1	0
F2	Fiber deliver 2	−117.4	0.5	0	0	1	0
M1	Mirror 1	66.3	−69.3	0	$\sqrt{2}/2$	$\sqrt{2}/2$	0
M2	Mirror 2	−106.9	86.4	0	$\sqrt{2}/2$	$-\sqrt{2}/2$	0
M3	Mirror 3	31.7	118.6	0	$-\sqrt{2}/2$	$-\sqrt{2}/2$	0
BS1	Beam splitter 1	103.2	−69.3	0	$-\sqrt{2}/2$	$\sqrt{2}/2$	0
BS2	Beam splitter 2	66.3	43.9	0	$-\sqrt{2}/2$	$-\sqrt{2}/2$	0
BS3	Beam splitter 3	0	43.9	0	$\sqrt{2}/2$	$-\sqrt{2}/2$	0
BS4	Beam splitter 4	0	118.6	0	$\sqrt{2}/2$	$\sqrt{2}/2$	0
BS5	Beam splitter 5	31.7	86.4	0	$-\sqrt{2}/2$	$\sqrt{2}/2$	0
TM	Test mass	0	0	−33	0	0	1
RB	Reference beam	−106.9	80	0	0	1	0
MB	Measurement beam	103.2	0	0	0	−1	0
QPD	QPDs	0	146.7	0	0	−1	0

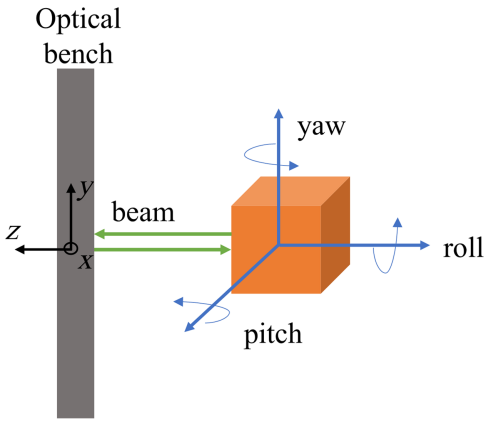

Fig. 2 Relative position of the optical bench and test mass with angle definitions: yaw, pitch, and roll. The measurement beam of the test mass interferometer enters through the center of the optical bench, propagates to the test mass surface, and then reflects back along the *z*-axis to the optical bench.

Based on the above simulation, a dataset for TTL-coupled noise analysis can be formed. The construction of input parameter space containing various influences is the first step. These parameters include the position, orientation, and attribute parameters of beams, optical components, test mass, and QPD. Setting the value range and sampling step for each parameter, the Latin hypercube sampling method is used to generate 10,000 input parameter combinations. The simulation program is run to obtain the LPS values corresponding to each set of input parameters.

3.2 XGBoost Model

Given the characteristics of TTL coupling noise, with its numerous influencing parameters and nonlinear correlation mechanism, a typical gradient-boosting machine learning framework, the

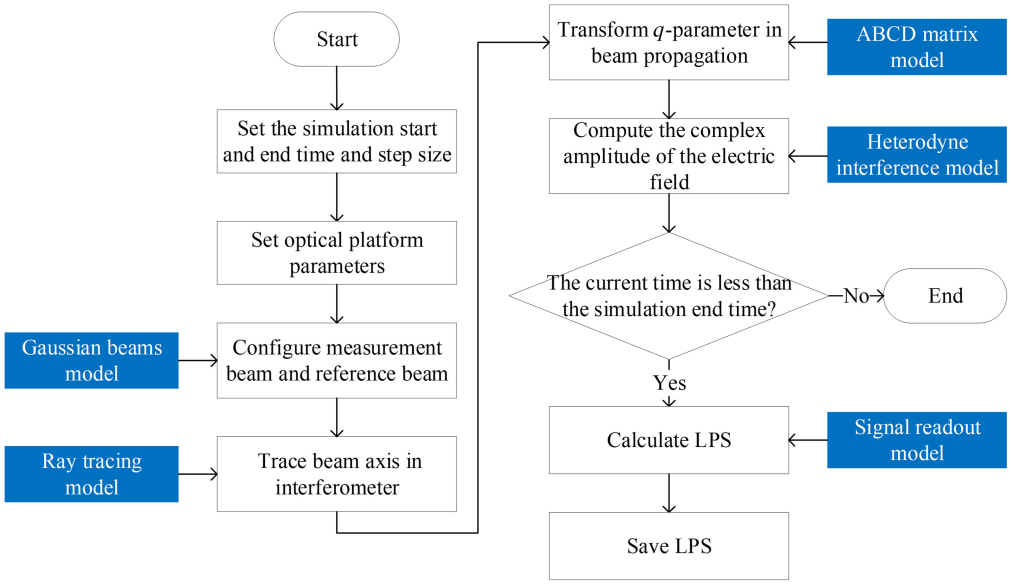

Fig. 3 Simulation flowchart of the test mass interferometer output.

XGBoost regression model, is employed in this study to model the relationships between the influencing parameters and LPS.

The objective function of XGBoost is defined as[21]

$$\text{obj} = \sum_i l(\text{LPS}_i^{\text{pred}}, \text{LPS}_i^{\text{truth}}) + \sum_t \Omega(f_n), \tag{5}$$

$$\Omega(f_n) = \gamma_1 N + \frac{1}{2}\gamma_2 \|w\|^2, \tag{6}$$

where $\text{LPS}_i^{\text{pred}}$ is the predicted LPS, $\text{LPS}_i^{\text{truth}}$ is the true LPS according to the data, and i is the i'th sample. l is the loss function, indicating the error between the real and predicted values, N is the number of leaves, f_n is the n'th tree, and γ_1 and γ_2 are regularization terms. The tree model splits the data based on input parameters into multiple groups, and each leaf score represents the predicted value for all the data points that fall into that specific leaf. A larger leaf score indicates a higher predicted value for the data, and w is a vector composed of leaf scores. $\Omega(f_n)$ indicates the complexity of the tree; the smaller the value, the less complex the tree, and the stronger the generalization ability of the model.

The R-squared value, also known as the coefficient of determination, is a measure indicating the goodness of fit of the data to the model. The R-squared value has a range of [0, 1], with 1 indicating a perfect fit. The R-squared value is calculated as

$$R^2 = 1 - \frac{\sum_i (\text{LPS}_i^{\text{pred}} - \text{LPS}_i^{\text{truth}})^2}{\sum_i (\text{LPS}_i^{\text{truth}} - \overline{\text{LPS}})^2}, \tag{7}$$

where $\overline{\text{LPS}}$ represents the average value of the LPS in the dataset.

3.3 SHAP Value

The XGBoost model is employed to fit the relationship between the angular misalignment parameters and LPS caused by the TTL coupling noise in the test mass interferometer. Although XGBoost can provide feature importance attribution values, such as gain, cover, and weight, these methods have inherent limitations and often lack sufficient interpretability.[23] When parameters affecting TTL coupling noise are incorporated into the XGBoost model, the input order of the parameters is random. This randomness can result in slight biases in the computed parameter sensitivity. In addition, because XGBoost is a tree-based model, the obtained parameter sensitivity is heuristic. Consequently, the sensitivity analysis should also include model interpretation methods.

The SHAP values come from cooperative game theory and have been applied in the field of machine learning to interpret why a model made a prediction. For a machine learning model f with a set of input parameters N, the purpose of the SHAP value is to assess the contribution of each parameter based on the different ways of parameter combination and their corresponding model outputs. This is realized by evaluating the impact on the output when a parameter is missing, also known as marginal contribution. Considering that there are many different parameter combinations, a reasonable weighting is introduced to synthesize the marginal contribution for all possible combinations. Of all the currently popular parameter attribution methods, SHAP values have been shown to be the only possible consistent, locally accurate method.[23]

To compute SHAP values, Lundberg et al. defined $f_x(S) = E[f(x)|x_s]$ to be the expected value of the function f conditioned on a subset S of the input parameter. The expression for the SHAP value is as follows:[23,24]

$$\phi_m = \sum_{S \subseteq N \setminus \{m\}} \frac{|S|!(M - |S| - 1)!}{M!} [f_x(S \cup \{m\}) - f_x(S)], \tag{8}$$

where m is the m'th noise influence parameter, S is the input parameter subset without m used in the XGBoost model, N represents the set of all input parameters, and M represents the number of input parameters. The term in the form of fraction within the summation symbols indicates the weight of the subset S, and the item in square brackets is the marginal contribution of parameter m. For applying the SHAP value to evaluate the contribution of the input parameters to the TTL coupling noise, the LPS predicted by the XGBoost model is set to $f_x(S)$. The SHAP values can range from negative infinity to positive infinity, indicating the extent of influence each TTL coupling noise influence parameter has on prediction results. A positive SHAP value indicates that the feature contributes positively to the model prediction results, and a negative value indicates that the feature contributes negatively to the model prediction results.

The global importance can be defined as the average absolute SHAP value of each parameter[25]

$$I_m = \frac{1}{W} \sum_{W} |\phi_m|, \tag{9}$$

where W is the number of samples and w is the w'th sample.

On the basis of single-factor sensitivity analysis, multi-factor sensitivity analysis is achieved by constructing a matrix of attribution values[23] Φ for evaluating the impact of multiple factors on the predicted value of LPS

$$\Phi = \begin{bmatrix} \phi_{1,1} & \phi_{1,2} & \cdots & \phi_{1,M} \\ \phi_{2,1} & \phi_{2,2} & \cdots & \phi_{2,M} \\ \vdots & \vdots & \ddots & \vdots \\ \phi_{M,1} & \phi_{M,2} & \cdots & \phi_{M,M} \end{bmatrix}. \tag{10}$$

The elements in the matrix are collectively referred to as SHAP interaction values. The values at the off-diagonal positions of the matrix are the interaction effects, and the values at the diagonal positions are the main effects of the parameters. Interaction effects and main effects together constitute the SHAP values of the parameters.

The calculation method of interaction effects is as follows[23]

$$\phi_{m,n} = \sum_{S \subseteq N \setminus \{m,n\}} \frac{|S|!(M - |S| - 2)!}{2(M - 1)!} \nabla_{mn}(S), m \neq n, \tag{11}$$

where

$$\nabla_{mn}(S) = f_x(S \cup \{m, n\}) - f_x(S \cup \{n\}) - [f_x(S \cup \{m\}) - f_x(S)]. \tag{12}$$

The main effect is defined as[23]

$$\phi_{m,m} = \phi_m - \sum_{m \neq n} \phi_{m,n}. \tag{13}$$

The process for determining the global importance is summarized as follows: First, for each sample, the marginal contribution of each combination of TTL parameters is calculated, then the SHAP values of the TTL parameters are derived by weighted summation, and finally, all samples in the dataset are aggregated to calculate the average absolute value of all TTL parameters to obtain the global importance. The calculation of the interaction effects is similar to the calculation of the SHAP values.

4 Results and Discussion

4.1 Parameter Settings

According to the ideal test mass interferometer shown in Fig. 1, parameters related to the TTL coupling noise were divided into four categories, beam parameters, mirror and beam splitter parameters, test mass parameters, and QPD parameters. The range of parameter values was based on the index requirements of Taiji-3.[26–28]

The categories, parameters, and ranges of the simulation parameters are shown in Table 2. The beam parameters include the waist radius and waist position of both the reference and measurement beams, as well as the beam offset. The optical components in the ideal test mass interferometer are mainly beam splitters and mirrors. The displacement and deflection caused by in-orbit temperature and gravity release[29] in these components can cause TTL coupling noise. Thus, we considered the rotation point offsets of the components from the specified position. During the space gravitational wave detection mission operation, the position and orientation of the test mass are always changing, obey dynamics laws, and also generate TTL coupling noise. The basic parameters of QPD include radius and slit size, which are considered in both simulation and analysis. A total of 60 parameters made up the parameter space simulated and analyzed in this paper.

4.2 Model Validation

To ensure the reliability of the machine learning results, this study utilizes the outcomes of analytical models as a validation benchmark. The analytical models are constructed based on the underlying physical principles.[19,22] The consistency and accuracy of the machine learning analysis can be verified by comparing the parameter importance rankings derived from the analytical models with the results obtained through machine learning.

The beam parameters include the beam waist radius, waist position, and beam offset. When considering the beam offset on the detector, the coupling of beam parameters is expressed as a

Table 2 Parameter information for the simulation and analysis of TTL coupling noise.

Categories	Parameter	Range
Beam parameters	Waist radius	(0.4 mm, 0.6 mm)
	Waist position	(−1 cm, 1 cm)
	Beam offset	(−10 μm, 10 μm)
Mirror and beam splitter parameters	Rotation point offset	(−100 μm, 100 μm)
	Angle	(−75 μrad, 75 μrad)
Test mass parameters	Angle	(−300 μrad, 300 μrad)
QPD parameters	Radius	(599.8 μm, 600.2 μm)
	Slit size	(9.8 μm, 10.2 μm)

combination of linear and second-order terms.[22] By omitting the second-order terms, the equation is as follows:

$$\mathrm{LPS_{ng}} \approx x_m \frac{z_{Rm}(z_{Rm}+z_{Rr})+z_m(z_m-z_r)}{(z_{Rm}+z_{Rr})^2+(z_m-z_r)^2}\varphi_m. \tag{14}$$

z_{Rm} and z_{Rr} represent the Rayleigh distances of the reference and measurement beam, respectively. z_m and z_r are the beam waist positions of the measurement and reference beam, respectively. x_m is the beam offset of the measurement beam, and φ_m is the rotation angle of the measurement beam.

The partial derivative of the waist radius of the measurement beam is

$$\partial \mathrm{LPS_{ng}}/\partial\omega_m = x_m\varphi_m \cdot \frac{2\omega_m\omega_r^2}{(\omega_m^2+\omega_r^2)^2}, \tag{15}$$

the partial derivative of the waist position of the measurement beam is

$$\partial \mathrm{LPS_{ng}}/\partial z_m = x_m \cdot \frac{4z_R^2 z_m - z_r(z_m-z_r)^2}{(4z_R^2+(z_m-z_r)^2)^2} \cdot \varphi_m, \tag{16}$$

the partial derivative of the measurement beam offset is

$$\partial \mathrm{LPS_{ng}}/\partial x_m = \varphi_m \frac{z_{Rm}(z_{Rm}+z_{Rr})+z_m(z_m-z_r)}{(z_{Rm}+z_{Rr})^2+(z_m-z_r)^2}. \tag{17}$$

Substituting the measured beam waist radius and position of 0.6 and 10 mm, respectively, along with the reference beam waist radius and position of 0.5 and 0 mm, the corresponding partial derivative values were calculated. The results indicate that $\partial(\mathrm{LPS_{ng}})/\partial(z_m) < \partial(\mathrm{LPS_{ng}})/\partial(w_m) < \partial(\mathrm{LPS_{ng}})/\partial(x_m) < \varphi_m$.

The rotation point offset and angle of the test mass introduce geometric TTL coupling, which can be categorized into the lever arm effect and the piston effect. The partial derivative of the angle is

$$\partial \mathrm{OPD}/\partial\varphi = 4 * d_{\mathrm{lever}}\varphi + 2d_{\mathrm{long}}\varphi + 2d_{\mathrm{lat}}, \tag{18}$$

where φ represents the rotation angle of test mass, d_{lever} represents the length of the lever arm, d_{long} represents the longitudinal offset of the test mass rotation point relative to the reflection point, and d_{lat} represents the lateral offset of the test mass rotation point relative to the reflection point or the lateral coordinate offset of the test mass.

The contribution of d_{lat} to OPD is the first-order term of angle, which is dominant. The partial derivative of d_{lat} yields

$$\partial \mathrm{OPD}/\partial d_{\mathrm{lat}} = 2\varphi. \tag{19}$$

It is obvious that the effect of the angle will be greater than that of lateral offset, i.e., $\partial(\mathrm{LPS})/\partial(\varphi) > \partial(\mathrm{LPS})/\partial(d_{\mathrm{lat}})$. In addition, the angle will be coupled with other parameters listed in Table 2, which is expected to cause a greater impact. As this study considers the angle in three dimensions, it is necessary to introduce the lever arm effect and piston effect in the 3D case

$$\partial \mathrm{OPD}^{3D}/\partial\eta \approx 2d_{\mathrm{vert}} + 2d_{\mathrm{long}}\eta + 4d_{\mathrm{lever}}\eta, \tag{20}$$

where η represents the pitch angle of the test mass and d_{vert} refers to the rotation point offset of the test mass in the y-direction. φ represents the yaw angle of the test mass in the 3D case. Formulaically, the only difference between the results of the derivation of η and the derivation of φ is the difference between d_{lat} and d_{vert}, but the effect is not as pronounced as that of φ due to the fact that d_{vert} is smaller than d_{lat} in the local dynamics model.[30] The analysis shows that the importance of the test mass TTL coupling parameters follows the order: $\varphi > \eta > d_{\mathrm{lat}} > d_{\mathrm{long}}$.

The TTL coupling generated by the QPD parameters originates from the combined contributions of an infinitely large single element photodiode (SEPD) and the geometric phase.[22] Among these, the TTL coupling produced by the infinitely large SEPD is dominant. Therefore, the influence of the QPD radius and the slit size on TTL coupling can be considered negligible.

The analytical model provides the importance of parameters within each category, as well as the ranking of their respective influence within the category. For the beam parameters, the beam offset has a greater influence than other beam parameters. For the test mass parameters, the angle of test mass and lateral coordinate offset exhibit the largest effects. Theoretically, the TTL coupling parameters of each mirror and beam splitter follow a similar ranking to the test mass parameters but have a smaller impact due to their narrower parameter range. The QPD parameters can be neglected. The analysis yields a ranking of the influence of parameters within each category. However, determining the relative importance of different parameter categories and understanding the interactions among them remains a significant challenge. The multi-factor coupling cannot be fully captured through analytical approaches. Therefore, a multi-factor sensitivity analysis is essential to provide a more robust framework for quantifying these interdependencies and obtaining a comprehensive characterization of the system's behavior.

4.3 Results of Parameter Sensitivity Analysis

According to the defined parameter space, the LPS values caused by TTL coupling noise were predicted using the XGBoost model, and sensitivity analysis was conducted by calculating the global importance.

The global importance of the key parameters calculated using the SHAP values is shown in Table 3. The rule for defining variables in the table is that z_a before the underline represents the angle around the z-axis, and the abbreviation after the underline represents the abbreviation of the component name corresponding to Table 1.

The larger the global importance of the key parameters, the more sensitive the TTL coupling noise is to changes in those parameters. Therefore, these parameters should be carefully controlled during instrument design to prevent the generation of excessive noise. The results indicate that the yaw angle of the test mass has the most significant impact on the TTL coupling noise, with a global importance of ∼0.23. Although the pitch angle and the lateral coordinate offset of the test mass are relevant to TTL noise, their impact is comparatively moderate, as reflected by SHAP values of 0.18 and 0.09, respectively. The test mass is in free suspension, and its position and attitude are always changing obeyed dynamics laws during space-based measurements. The angle and coordinate offset of the test mass induces lever arm, piston effects, and beam offset on the QPD, resulting in variations in the optical path length and additional phase changes. In the design of the interferometric measurement system, the disturbance reduction system is used for controlling the angular and coordinate changes of the test mass.[31] To effectively suppress the TTL coupling noise, it is essential to limit these changes, which in turn imposes requirements on the

Table 3 Global importance for various influencing factors of TTL coupling noise.

Variable	Meaning	Global importance
φ_TM	Yaw angle of TM	0.231
η_TM	Pitch angle of TM	0.184
$d_{\text{lat\_TM}}$	Lateral coordinate offset of TM	0.087
z_{a_M3}	Angle of M3 (z- axis)	0.076
z_{a_BS1}	Angle of BS1 (z- axis)	0.066
z_{a_M2}	Angle of M2 (z- axis)	0.065
z_{a_BS4}	Angle of BS4 (z- axis)	0.064
z_{a_M1}	Angle of M3 (z- axis)	0.062
z_{a_BS5}	Angle of BS5 (z- axis)	0.060
z_{a_BS3}	Angle of BS3 (z- axis)	0.058
z_{a_BS2}	Angle of BS2 (z- axis)	0.057

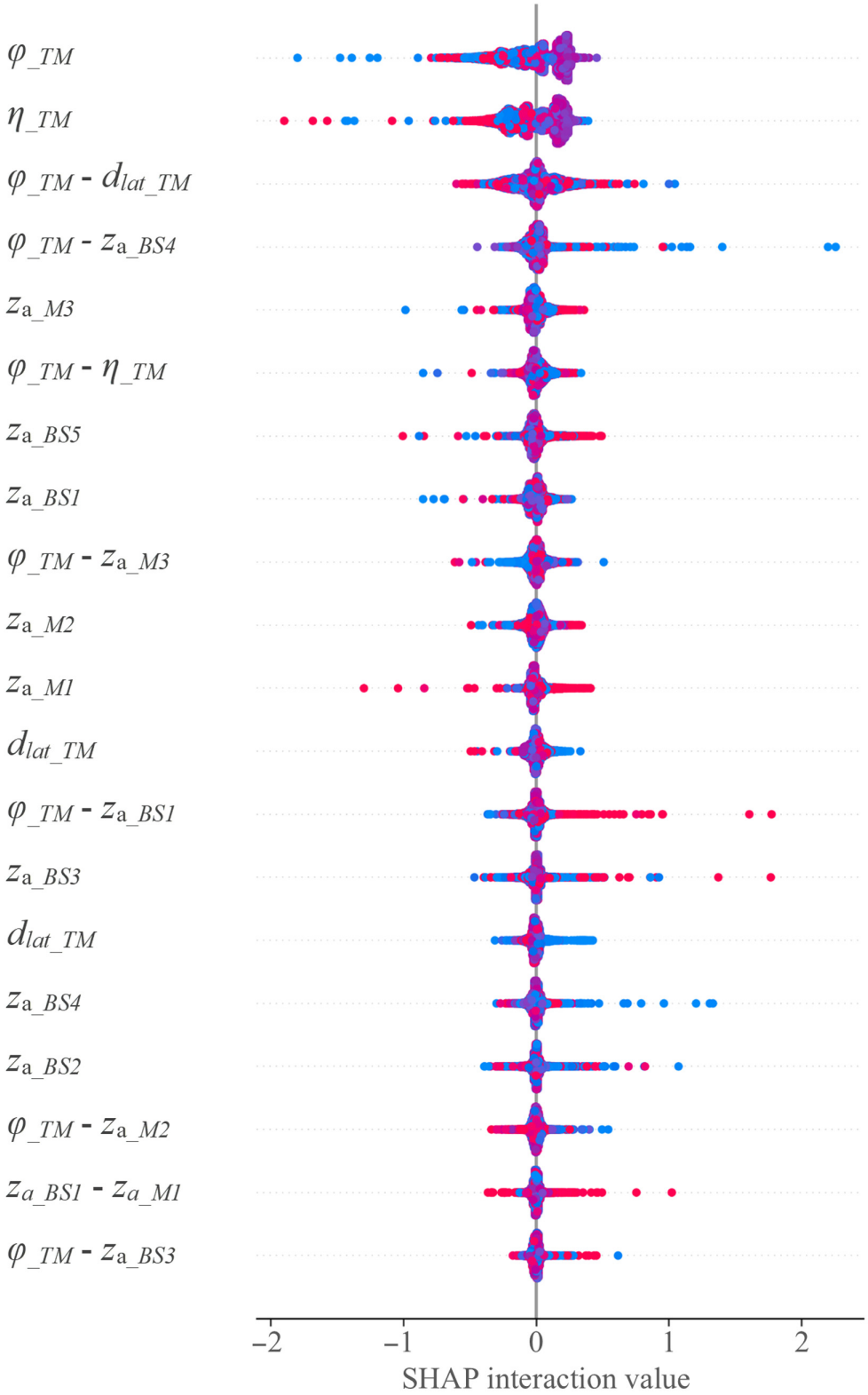

Fig. 4 Ranking of SHAP interaction values. The left side of the figure shows the parameters or interaction parameters. From top to bottom, the main effects or interaction effects are arranged in descending order.

design of the disturbance suppression system. The angle around z-axis of mirrors and beam splitters also affects the optical path moderately, with global importance of ∼0.1. For mirrors and beam splitters, there are dynamic random angle variations due to in-orbit temperature and gravity release, which in turn cause lever arm effects and beam offset on the QPD. Therefore, choosing appropriate materials for optical components and maintaining precise temperature control are essential for effectively suppressing TTL coupling noise.

Figure 4 shows the ranking of SHAP interaction values. Each row consists of 10,000 data points, representing the sample size of the dataset. The width of the positions in the figure indicates a large concentration of data samples, with wider subplots indicating greater effects on noise, whether it be main effects or interaction effects. Parameters displayed individually represent the main effects, whereas interaction effects are indicated when parameters are displayed together. For example, when φ_TM is displayed alone, it represents the main effect of the yaw angle of TM. However, when φ_TM − <some other parameter> is displayed, it represents the interaction effect between φ_TM and the other parameter, capturing how their combined influence contributes to the TTL coupling noise. The color of the data points represents different effects, with red indicating positive changes in parameters and blue indicating negative changes. From the figure, it is apparent that parameters related to the angle have a significant impact on TTL coupling noise and exhibit varying directions of influence. In addition to the strong influence of a single parameter on the TTL coupling noise, key parameters that have significant impacts on TTL coupling noise (as shown in Table 3) coupled to the yaw angle of test mass also contribute significantly to the TTL coupling noise. Moreover, the interaction effects of angular parameters have more influence on the TTL coupling noise than parameters such as the beam and QPD. Therefore, during the suppression of TTL coupling noise, particular attention should be placed on the angle of test mass, which provides design constraints for the disturbance reduction system.

The sensitivity analysis conducted using machine learning demonstrates consistency with the analytical model, especially in identifying the dominant parameters influencing the TTL coupling. Moreover, the machine learning model offers additional capabilities that go beyond the scope of traditional analytical methods, particularly when it comes to the contributions of parameters from different categories and higher-order interactions, which are difficult to derive from analytical models. The global importance results show that the test mass parameters have the greatest influence, followed by the parameters related to the mirrors and beam splitters. Specifically, the angles of the mirrors and beam splitters around the z-axis have a comparable impact on the lateral coordinate offset of the test mass. The influence of beam parameters can be considered negligible in the overall sensitivity analysis. In addition, analysis using SHAP interaction values indicates that the coupling between the yaw angle of test mass and the angles of mirrors or beam splitters around the z-axis contributes significantly to TTL coupling. These findings highlight the advantage of machine learning in uncovering complex relationships and parameter interactions that may be challenging to derive through traditional analytical methods.

After retaining the top 11 parameters, the R-squared value stabilizes at ∼0.8, demonstrating that the XGBoost model can still effectively fit the relationship between key parameters and TTL coupling noise, even after removing redundant parameters.

5 Conclusion

Based on Gaussian beam, ray tracing, ABCD matrix, heterodyne interference, and QPD signal readout models, the test mass interferometer for the Taiji program was simulated to generate the LPS data caused by TTL coupling noise. Linear and nonlinear relationships among parameters and LPS were fitted using the XGBoost model. The SHAP values were used to interpret the XGBoost model results and were compared with the expected results from the analytical models. Then, the parameter space was reduced from ∼60 to 11 dimensions, retaining parameters related to the angle and coordinate.

The sensitivity analysis using machine learning aligns with the analytical model and provides additional insights, especially regarding the contributions of different parameter categories and higher-order interactions. The analysis results revealed that the yaw angle of the test mass had the most significant impact on the TTL coupling noise, followed by the pitch angle of the

wtest mass. Although the influence of the angle of beam splitters and mirrors around the z-axis and lateral coordinate offset of test mass is somewhat lesser than that of the angle, it is still considerably more substantial than that of the remaining parameters. Furthermore, the interactions between the angle of the test mass and other key parameters had a significant impact on the noise.

These results suggest that future experiments should focus on angular-related parameters, especially the angle of the test mass and that of mirror and beam splitters. This study employs machine learning techniques to identify the key parameters influencing TTL coupling noise, which provides design constraints for the interferometric measurement system and the disturbance reduction system. Moreover, the method effectively addresses the issue of algorithmic nonconvergence due to an excessive number of optimization parameters.

Disclosures

The authors declare that there are no financial interests, commercial affiliations, or other potential conflicts of interest that could have influenced the objectivity of this research or the writing of this paper.

Code and Data Availability

Data underlying the results presented in this paper are not publicly available at this time but may be obtained from the authors upon reasonable request.

Acknowledgments

This work was funded by the National Key Research and Development Program of China (Grant No. 2020YFC2200100) and the Chinese Academy of Sciences Strategic Pioneer Program on Space Science (Grant No. XDA1502110201).

References

1. M. Colpi et al., "LISA study definition report," ESA (2023).
2. S. Cao et al., "DECi-hertz interferometer gravitational-wave observatory: forecast constraints on the cosmic curvature with LSST strong lenses," *Astrophys. J.* **926**(2), 214 (2022).
3. J. Luo et al., "TianQin: a space-borne gravitational wave detector," *Class. Quantum Grav.* **33**(3), 035010 (2016).
4. W. Hu and Y. Wu, "The Taiji Program in Space for gravitational wave physics and the nature of gravity," *Natl. Sci. Rev.* **4**(5), 685–686 (2017).
5. K. Danzmann et al., "LISA assessment study report," ESA (2011).
6. S. Schuster, *Tilt-to-Length Coupling and Diffraction Aspects in Satellite Interferometry*, Gottfried Wilhelm Leibniz Universität Hannover (2017).
7. H. Wegener et al., "Tilt-to-length coupling in the grace follow-on laser ranging interferometer," *J. Spacecraft Rockets* **57**(6), 1362–1372 (2020).
8. C. P. Sasso, G. Mana, and S. Mottini, "Coupling of wavefront errors and jitter in the LISA interferometer: far-field propagation," *Class. Quantum Grav.* **35**(18), 185013 (2018).
9. C. P. Sasso, G. Mana, and S. Mottini, "Coupling of wavefront errors and pointing jitter in the LISA interferometer: misalignments of the interfering wavefronts," *Class. Quantum Grav.* **35**(24), 245002 (2018).
10. C. P. Sasso, G. Mana, and S. Mottini, "Telescope jitters and phase noise in the LISA interferometer," *Opt. Express* **27**(12), 16855 (2019).
11. Y.-Z. Tao, H.-B. Jin, and Y.-L. Wu, "The estimation of far-field wavefront error of tilt-to-length distortion coupling in space-based gravitational wave detection," *Chinese Phys. B* **32**(2), 024212 (2023).
12. Z. Wang et al., "Alternative approach to tilt-to-length coupling estimation for laser ranging interferometers in future gravity missions," *Remote Sens.* **16**(5), 862 (2024).
13. J. Li et al., "Evaluation method for the design results of space gravitational-wave telescopes," *Meas. Sci. Technol.* **34**(5), 055409 (2023).
14. X. Cui, C. Fang, and Z. Wang, "Influence of installation and adjustment error of gravitational wave telescope on TTL noise," *Acta Opt. Sin.* **43**(19), 1912001 (2023).
15. M. Tröbs et al., "Reducing tilt-to-length coupling for the LISA test mass interferometer," *Class. Quantum Grav.* **35**(10), 105001 (2018).
16. M.-S. Hartig and G. Wanner, "Tilt-to-length coupling in LISA pathfinder: analytical modelling," *Phys. Rev. D* **108**(2), 022008 (2023).

17. M. Armano et al., "Tilt-to-length coupling in LISA pathfinder: a data analysis," *Phys. Rev. D* **108**(10), 102003 (2023).
18. G. Wanner et al., "In-depth modeling of tilt-to-length coupling in LISA's interferometers and TDI Michelson observables," *Phys. Rev. D* **110**(2), 022003 (2024).
19. M.-S. Hartig, S. Schuster, and G. Wanner, "Geometric tilt-to-length coupling in precision interferometry: mechanisms and analytical descriptions," *J. Opt.* **24**(6), 065601 (2022).
20. Z. Luo et al., "A brief analysis to Taiji: science and technology," *Results Phys.* **16**, 102918 (2020).
21. T. Chen and C. Guestrin, "XGBoost: a scalable tree boosting system," in *Proc. 22nd ACM SIGKDD Int. Conf. Knowl. Discov. and Data Mining*, ACM, San Francisco, California, USA, pp. 785–794 (2016).
22. M.-S. Hartig et al., "Non-geometric tilt-to-length coupling in precision interferometry: mechanisms and analytical descriptions," *J. Opt.* **25**(5), 055601 (2023).
23. S. M. Lundberg, G. G. Erion, and S.-I. Lee, "Consistent individualized feature attribution for tree ensembles," arXiv:1802.03888 (2019).
24. C. Molnar, *Interpretable Machine Learning: A Guide for Making Black Box Models Explainable*, Leanpub, Victoria, British Columbia (2020).
25. I. C. Covert, S. Lundberg, and S.-I. Lee, "Understanding global feature contributions with additive importance measures," in *Adv. in Neural Inf. Process. Syst.*, Vol. 33, pp. 17212–17223 (2020).
26. M. Zhao et al., "Preliminary simulation of intersatellite laser interference link for the Taiji program," *J. Astron. Telesc. Instrum. Syst.* **8**(3), 038002 (2022).
27. Y. Zhao, *The Research on the Tilt to Length Coupling Noise in Inter-Satellite Interference Link for the Space-Based Gravitational Wave Detection*, University of Chinese Academy of Sciences (2021).
28. W. Tao et al., "Design and construction of the optical bench interferometer for the Taiji program," *Sensors* **23**(22), 9141 (2023).
29. W. Zhi et al., "Preliminary design and analysis of telescope for space gravitational wave detection," *Chinese Opt.* **11**(1), 131–151 (2018).
30. S. Vidano et al., "The LISA DFACS: model predictive control design for the test mass release phase," *Acta Astronautica* **193**, 731–743 (2022).
31. O. Jennrich, "LISA technology and instrumentation," *Class. Quantum Grav.* **26**(15), 153001 (2009).

Fei Xie is a PhD candidate at the University of Chinese Academy of Sciences. She graduated from Ningbo University in 2020. Her research interests focus on the simulation and optimization of space gravitational wave laser interferometry simulation systems.

Xiaodong Peng is a professor at the National Space Science Center of the Chinese Academy of Sciences. He received his PhD degree from the Graduate School of the Chinese Academy of Sciences. His research interests focus on high-precision simulation and evaluation of space missions and intelligent analysis and prediction of space big data.

Wenlin Tang is a professor at the National Space Science Center of the Chinese Academy of Sciences. He received his PhD from the Institute of Mathematics and Systems Science of the Chinese Academy of Sciences. His research interests focus on space gravitational wave detection and complex system simulation.

Mengyuan Zhao is a lecturer at Xi'an University of Finance and Economics. She received her PhD from the National Space Science Center of the Chinese Academy of Sciences. Her research interests focus on complex system simulation.

Xiaoshan Ma is a professor at the Institute of Engineering Thermophysics, Chinese Academy of Sciences. She received her PhD from the Hefei Institutes of Physical Science, Chinese Academy of Sciences. Her research interests focus on complex system simulation.